Hydrogen passivation of the selenium double donor in silicon: A study by magnetic resonance

P. T. Huy
Van der Waals–Zeeman Institute, University of Amsterdam, Valckenierstraat 65, NL-1018 XE Amsterdam, The Netherlands and International Training Institute for Materials Science, ITIMS Building, Dai hoc Bach Khoa Hanoi, 1 Dai Co Viet Road, Hanoi, Vietnam

C. A. J. Ammerlaan and T. Gregorkiewicz
Van der Waals–Zeeman Institute, University of Amsterdam, Valckenierstraat 65, NL-1018 XE Amsterdam, The Netherlands

D. T. Don
Faculty of Physics, University of Hanoi, 92 Nguyen Trai, Hanoi, Vietnam
(Received 27 July 1999; revised manuscript received 29 October 1999)

The passivation by hydrogen of selenium double donors in silicon has been investigated by magnetic resonance. Hydrogen was introduced by heat treatment at high temperatures in an atmosphere of water vapor. Two spectra were observed, labeled Si-NL60 and Si-NL61 for further reference, both showing trigonal symmetry for the paramagnetic center. By using isotopically enriched selenium and heavy (deuterated) water, the participation of selenium and hydrogen in the structure of the centers was conclusively established. By analysis of the experimental data, microscopic models for the centers were developed. It is concluded that spectrum Si-NL60 corresponds to a SeH pair in a neutral charge state. An unambiguous interpretation of the Si-NL61 spectrum cannot yet be presented. According to the spectroscopic information from the experiment, Si-NL61 is the spectrum of a selenium center with two hydrogen atoms on nonequivalent sites, which is observed in an ionized state. Alternatively, it could correspond to two neutral one-selenium–one-hydrogen pairs which resemble each other so much that they are indistinguishable by electron paramagnetic resonance.

I. INTRODUCTION

In recent years the chalcogen elements—sulfur, selenium, and tellurium—as dopant impurities in silicon have been subjected to intensive investigations, both by experiment and theory. As a result the microstructure of these electronic centers and their properties are well established. The chalcogen impurities occupy substitutional sites in the crystalline silicon. Electronically they behave as double donors, though with deep levels for both first and second ionization processes.[1,2] The chalcogen impurities have shown a strong tendency to be involved in complex formation. They easily form complexes among themselves of homonuclear type, such as S_2 and Se_2, or of a heteronuclear structure as for instance SSe.[3] Complex formation between chalcogen atoms and other impurities, e.g., iron and copper, has been reported as well.[4–8] In this perspective the interaction of chalcogen atoms with hydrogen, also known for its reactivity, is an interesting field for study. The issue is of practical technological relevance, as the presence of hydrogen in crystalline semiconductors has been shown to cause significant changes in the properties—electrical, optical, etc.—of the material. Hydrogen passivation of electrically active centers has become an engineering tool. Early observations demonstrated the passivation of shallow single acceptor and donor impurities in silicon.[9,10] Also, neutral centers can bind hydrogen and become electronically active centers. A most interesting example in this category is the isoelectronic carbon impurity.[11] Double donors are another interesting category of impurity, as, due to their electronic structure, the effect of partial passivation is likely to occur, possibly correlated with the binding of one or more hydrogen atoms.

Passivation studies on all three chalcogen double donors, using the experimental technique of deep-level transient spectroscopy, were carried out by Pensl and co-workers.[12,13] They found that hydrogenation fully passivated the donors, i.e., both band-gap levels were removed, no new levels were introduced. In later experiments carried out by Peale *et al.* using infrared-absorption spectroscopy, three donor levels related to sulfur-hydrogen centers were identified.[14] Stimulated by this apparent controversy the magnetic resonance technique has been applied more recently on sulfur-doped silicon. In these studies two spectra, known as Si-NL54 and Si-NL55, were identified as arising from two structurally different impurity pairs of substitutional sulfur and interstitial hydrogen in the neutral charge state.[15,16] Samples in which the two magnetic resonance spectra were observed also showed the presence of the three infrared-absorption spectra,[17] on the one hand providing mutual support but on the other hand indicating that the correlation between the two techniques is not known in full detail. Formation of analogous complexes is anticipated for the two other chalcogen elements.

In this paper, we therefore report on a study of hydrogen passivation of the selenium double donor in silicon. The method of magnetic resonance, in its varieties of electron paramagnetic resonance (EPR) and the double-resonance techniques of electron-nuclear double resonance (ENDOR) and field-scanned ENDOR (FSE), has been applied. Magnetic resonance has proven itself to be a most suitable tool for identification and further characterization of the chalcogen impurities in single isolated[4,18–20] or complexed

forms,[21–23] as well as for chalcogen-impurity complexes.[4,5,8] The observation of two EPR centers, labeled Si-NL60 and Si-NL61, corresponding to two different selenium-hydrogen complexes, will be reported.

II. SAMPLE PREPARATION AND EXPERIMENTAL APPARATUS

The samples were prepared by thermal diffusion of natural selenium, having 7.6% of the magnetic isotope ^{77}Se, or of selenium enriched to 99.1% in ^{77}Se into the starting material which was *p*-type float-zoned silicon doped with boron to the room temperature resistivity between 75 and 125 Ω cm. The samples, shaped as a rectangular bar with the typical dimensions $2\times2\times15\,\mathrm{mm}^3$, were enclosed in quartz ampoules together with 0.5–1 mg of selenium powder mixed with an excess amount of silicon powder to create a SiSe atmosphere. They were heated to 1350 °C for a period of 120–360 h. After the diffusion the rough surface layers of the samples were mechanically removed and the samples were etched in CP6 solution (HNO_3:HF:CH_3COOH=2:1:1). Hydrogen or deuterium was introduced in a high-temperature treatment, at 1250–1350 °C, in water vapor for 30–45 min, followed by a rapid quench to room temperature. Before measuring, all samples were once again etched in the CP6 solution.

Magnetic-resonance experiments were carried out using a superheterodyne spectrometer operated in the *K* band with the frequency near 23 GHz. Signals were observed with the spectrometer tuned to dispersion under conditions of adiabatic fast passage. The magnetic field was modulated to a depth below around 0.1 mT with a frequency of 175 Hz. To allow double-phase-sensitive detection of ENDOR signals, the rf field inducing the ENDOR transitions was modulated, on and off at the rate of 3.3 Hz. The spectrometer has an option of operation under full computer control. It is equipped with facilities for ENDOR and FSE measurements. In the latter mode, the magnetic field is scanned through the EPR condition while the rf is varied in such a way that the NMR condition remains satisfied. For a more complete description of the equipment and the experimental techniques, see, e.g., Ref. 24.

III. RESULTS

A. EPR spectrum

In the samples diffused with natural selenium the EPR spectra of single isolated selenium and of the selenium pair were detected at an observation temperature of 4.2 K. The intensity of these resonances was found to depend strongly on the quenching speed after selenium diffusion. A fast quench favors the creation of the isolated selenium centers. The spectra are not shown because of their generally low intensity, which possibly is due to full ionization of the donors in the *p*-type material. The spectra are identified as arising from Se^+ and $(Se_2)^+$ by their known *g* tensors and selenium hyperfine splittings. They are clearly different from the new spectra Si-NL60 and Si-NL61 to be reported.

After the hydrogen introduction treatment the selenium spectra are replaced by new resonances. A typical result recorded at the temperature $T=1.5$ K with the magnetic field *B* oriented along a crystallographic ⟨100⟩ direction is depicted in Fig. 1. The spectrum is interpreted as selenium related. In that view the strong central line corresponds to centers with the selenium isotopes with a zero nuclear spin *I*, whereas the two outermost pairs of lower-intensity satellites are from centers with the ^{77}Se isotope, having $I=\frac{1}{2}$. The relative intensity of the side lines to the central line is consistent with the 7.6% natural abundance of this isotope. The pair of very weak resonances indicated by arrows was detectable for some magnetic-field directions only. They might as well correspond to a selenium-related center, but no study of them was made. Also the spectral lines 1, 2, and 3, which were always found to exist, will not be discussed at this stage.

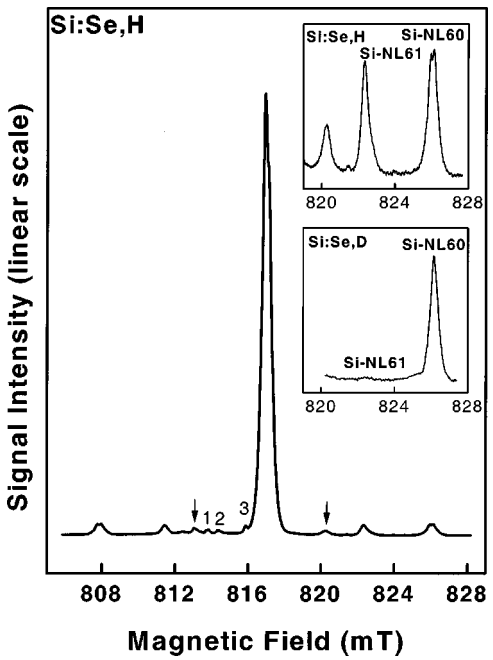

FIG. 1. EPR over the full field range of the Si-NL60 and Si-NL61 centers for the magnetic-field $B\|\langle100\rangle$ crystallographic direction, temperature $T=1.5$ K, and microwave frequency $f=22.8153$ GHz. The upper and lower insets show the structure of the high-field hyperfine satellite lines in samples doped with hydrogen and deuterium, respectively.

As shown on an expanded magnetic field scale in Figs. 2(a)–2(c), the central line has a multicomponent structure. The *g*-tensor anisotropy indicates a center symmetry lower than cubic. The resolution in EPR is, however, insufficient to reveal individual components and angular patterns. In spite of this handicap it appears that the linewidth and structure observed for hydrogenated and deuterated samples are different. This hints at a hydrogen involvement. In agreement with such an interpretation the linewidth in the deuterium spectrum is smaller. The insets of Fig. 1 show the structure of the high-field satellite lines in greater detail. Lines are labeled Si-NL60 and Si-NL61, respectively, as they belong to different independent spectra. As can be observed by comparing upper and lower insets the ratio of the intensities of the spectra can be vastly different in differently prepared samples. For the Si-NL60 spectrum a twofold splitting is apparent in the hydrogenated sample, and corresponds to a hydrogen hyperfine interaction which is just resolvable. For the deuterated sample (lower inset) the hyperfine splitting,

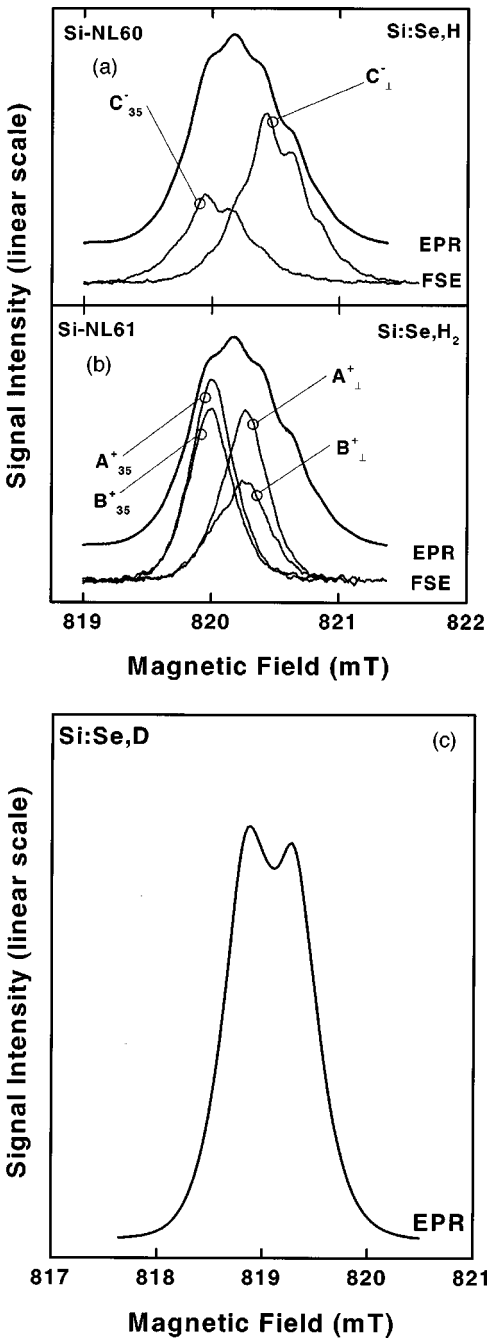

FIG. 2. Central part of the EPR spectrum (thick curves) for $B\|\langle 011\rangle$ on an expanded field scale. Components as resolved by FSE (thinner curves) indicate a center symmetry lower than cubic. Labels $A_{\perp}^{+}$, etc., specify the hydrogen ENDOR transitions selected for FSE. The line width and structure for hydrogenated [(a) and (b)] and deuterated (c) samples are different.

which must be ≈6.5 times smaller, is not visible. For the Si-NL61 spectrum any hydrogen hyperfine interaction will be smaller, as no splitting is observed in EPR. It has been possible to measure the full angular dependence of the hyperfine components of the spectra. The result, as shown in Fig. 3, reveals trigonal symmetry for both centers. Accidentally the g and A tensors give an equal anisotropy resulting in the quasi-isotropic behavior of the hyperfine lines on the high-field side, where the two interactions act in opposite senses.

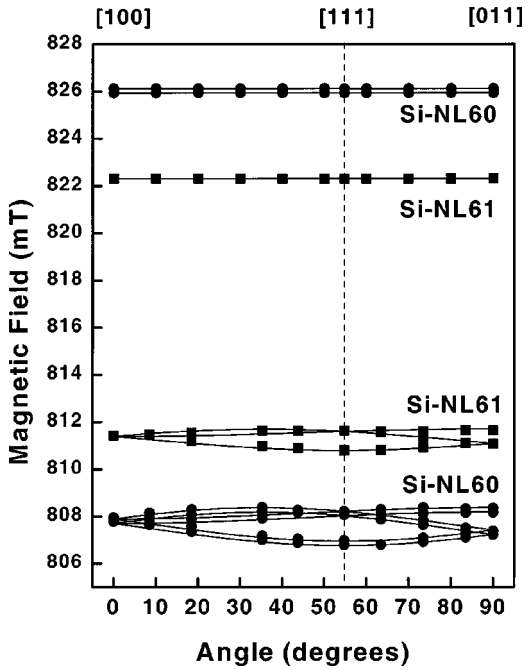

FIG. 3. Angular dependence of the Si-NL60 and Si-NL61 spectra of the ^{77}Se hyperfine lines, temperature $T=1.5$ K, microwave frequency $f=22.8252$ GHz. Experimental data: ■, ●. Solid lines are computer fits using the spin Hamiltonian described in Eq. (1). The double loops observed for the Si-NL60 center are due to hydrogen hyperfine interaction.

B. Hydrogen identification

For further study of the spectra, the ENDOR technique was applied. Following from the sample preparation the participation of hydrogen in the paramagnetic centers is anticipated. For that reason the range of hydrogen interaction frequencies has been carefully examined. With the magnetic field coincident with the central component of the EPR spectrum, i.e., at $B\approx 820$ mT, the ENDOR transitions are expected to be near the hydrogen nuclear Zeeman frequency $(\nu_Z)_H=(g_n)_H\mu_N B/h\approx 35$ MHz. For the proton the nuclear g value $(g_n)_H=5.585\,56$.[25] As shown in Fig. 4, indeed several ENDOR lines are observed in this frequency range with a pair-wise symmetrical displacement with respect to the hydrogen nuclear frequency. ENDOR spectra as shown in Fig. 4 were observed for several samples at slightly different values of the magnetic field for EPR, and therefore also slightly different frequencies for the ENDOR transitions. From the variation of the ENDOR frequencies with magnetic field, measured as ≈42 MHz/T and given by $d\nu/dB=g_n\mu_N/h$, all ENDOR lines are directly identified as arising from hydrogen. For these ENDOR spectra the complete angular dependence was as well obtained for the rotation of the magnetic field around a $\langle 011\rangle$ direction of the silicon crystal. Results are shown in Figs. 5(a) and 5(b) for the smaller and larger hyperfine splittings, respectively. The rotational patterns indicate trigonal symmetry of the underlying centers. As three patterns are observed, on either side of the nuclear frequency, with distinct hyperfine interactions three different hydrogen atoms must be present. For the larger hyperfine interaction the resonances for $B\|[100]$ do not exactly coincide. This is due to a small misalignment of this sample. The four lines as observed for an arbitrary angle of B correspond

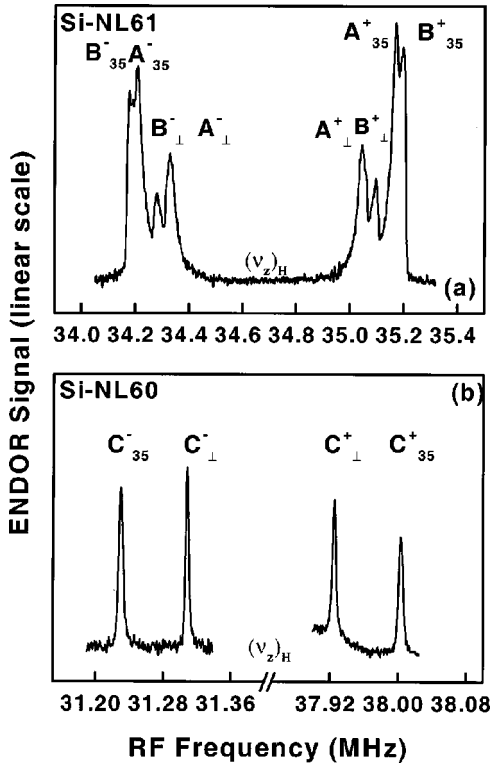

FIG. 4. Hydrogen ENDOR observed on the central line in the EPR spectrum, (a) close to proton Zeeman frequency $(\nu_Z)_H$ and (b) more distant from $(\nu_Z)_H$. The ENDOR transitions of different patterns for three hydrogen atoms are labeled *A* and *B* for the Si-NL61 center and *C* for Si-NL60. ENDOR frequencies are symmetrically displaced with respect to the hydrogen nuclear frequency. Magnetic field $B\|\langle 011\rangle$.

in a one-to-one manner with the four EPR orientations of the $\langle 111\rangle$-axial center. The magnitude of this hyperfine interaction is around 6.7 MHz. In EPR such a hyperfine strength gives a splitting of 0.24 mT, which is as observed for the spectrum labeled Si-NL60 in Figs. 1 and 3. It links the hydrogen and selenium hyperfine interactions to the same center. Also, for the deuterated samples the ENDOR spectra have been taken. Following from $(g_n)_D=0.857\,42$ (Ref. 25) for the deuteron the spectra are found near $(\nu_Z)_D=5.3$ MHz. An example of such ENDOR is given in Fig. 6. The angular variation of the deuterium hyperfine coupling shown in Fig. 7 agrees with the already established $\langle 111\rangle$-axial symmetry of the defect structure. Again, the mirror symmetry of the spectrum with respect to the Zeeman frequency of deuterium proves that the deuteron is the origin of the interaction. Due to the nuclear spin $I_D=1$, the number of transitions has doubled. The transitions $m_I=-1$ to $m_I=0$ and $m_I=0$ to $m_I=+1$ are split by the quadrupole effect, which is effective for this center of the axial symmetry. The frequencies for hydrogen and deuterium scale properly according to the ratio of their nuclear g values $(g_n)_H/(g_n)_D=6.5144$. Deuterium ENDOR corresponding to the lower of the hydrogen frequencies was not observed, as it is too close to the Zeeman frequency.

Having collected the ENDOR data all on the central line in the EPR spectrum with its unresolved structure, it remains to establish in more detail with which EPR transitions they are associated. For this goal the procedure of field-scanned

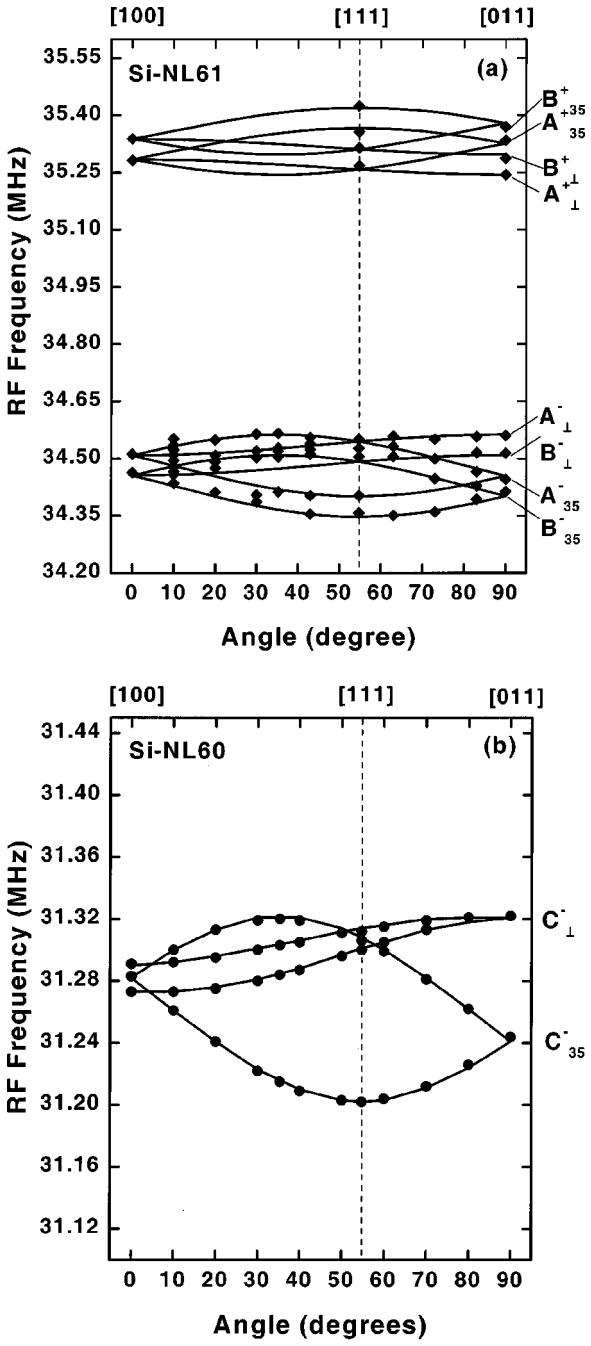

FIG. 5. Angular dependence of the hydrogen ENDOR spectra as observed for rotation of the magnetic field in the $(01\bar{1})$ plane from [100] to [011]. Results are shown in (a) for the smaller, and in (b) for the larger hyperfine splittings. Measurement conditions are temperature $T=9$ K, microwave frequency $f=22.909$ GHz, and magnetic field $B=814.812$ mT (a), and $T=8.2$ K, $f=22.7067$ GHz, and $B=813.168$ mT in (b).

ENDOR (FSE) is available. In an FSE scan the radio frequency remains locked to a selected NMR transition of ENDOR, even when the magnetic field is scanned to trace the EPR part of the double resonance. By the choice of an ENDOR frequency an impurity and the defect to which this impurity belongs are selected. Also specific defect orientations can be tagged and observed. FSE scans through the central region of the EPR were made for directions of *B* parallel to [100], [111], and [011]. The selected ENDOR

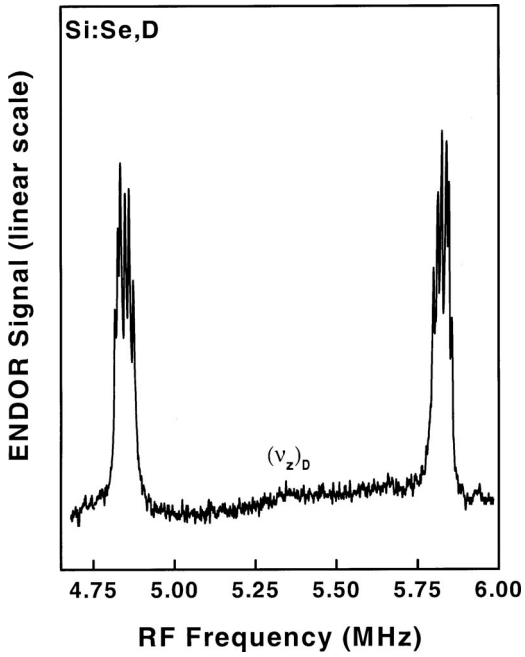

FIG. 6. Deuterium ENDOR observed on the central line of spectrum NL60 for $B=816.193$ mT in a direction about 20° away from [100] in the $(01\bar{1})$ plane. The nuclear Zeeman frequency of deuterium is $(\nu_Z)_D=5.334$ MHz.

transitions with $B\|[011]$ are labeled in Fig. 5 by *A*,*B*, and *C* for the three different hydrogen patterns, with a subscript indicating the angle between the [011] direction and the defect axis. Superscripts + and − distinguish between frequencies above and below the hydrogen Larmor frequency. The

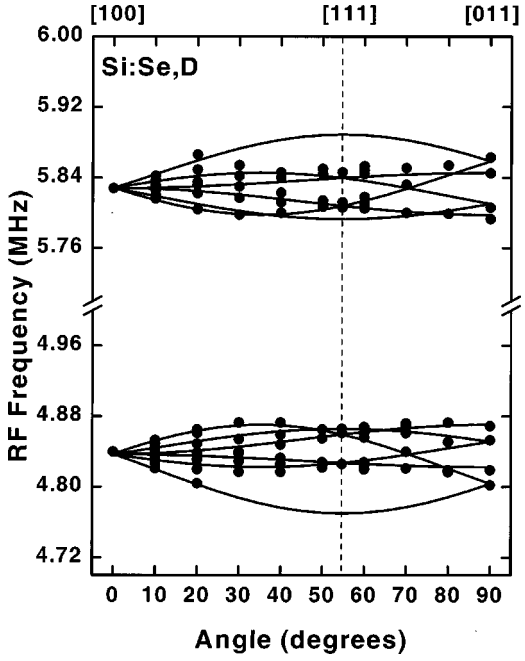

FIG. 7. Angular dependence of the deuterium ENDOR of spectrum Si-NL60 for rotation of the magnetic field in the $(01\bar{1})$ plane from [100] to [011]. Experimental data (●) are presented together with computer fitting (solid lines). Temperature $T=5.2$ K, microwave frequency $f=22.7994$ GHz, and magnetic field $B=816.193$ mT.

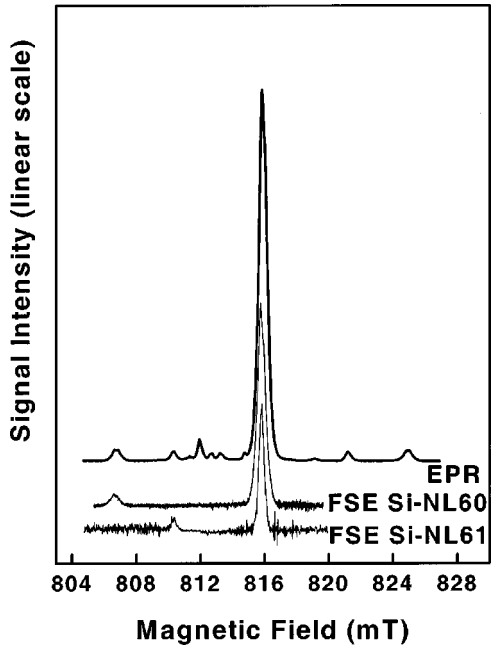

FIG. 8. EPR and FSE scans over a range of magnetic field also covering the regions of selenium hyperfine splitting. FSE Si-NL61 is observed on hydrogen ENDOR frequencies *A* and *B*; FSE Si-NL60 is related to the *C* hydrogen ENDOR. Magnetic field $B\|\langle 100\rangle$.

FSE spectra as obtained are shown in Figs. 2(a) and 2(b), and it is seen that they form components of the resonance line as observed in EPR. The result suggests that with FSE the structure of the central line is fully resolved. For the *A* and *B* hydrogen atoms the resonance lines coincide, indicating equal *g* tensors for the centers of these atoms. Hydrogen atom *C* generates FSE lines at somewhat higher fields, and belongs to a center with a different *g* tensor. The two peaks are the result of the hydrogen hyperfine coupling of around 6.7 MHz in ENDOR and 0.24 mT in EPR. For the *A* and *B* hydrogen atoms a hyperfine interaction constant of around 0.8 MHz leads to an EPR splitting of 0.03 mT, which is too small compared to the linewidth to be observable. The angular dependence pattern based on FSE measurements confirms the trigonal symmetry of the centers. From the data obtained by FSE, the two *g* tensors are determined.

FSE scans were also made over a wider range of magnetic fields covering the regions of selenium hyperfine split lines as presented in Fig. 1 as well. From an inspection of the spectra shown in Fig. 8 one concludes that with the *C* hydrogen atom only the selenium atom with the wider doublet splitting, labeled Si-NL60, is related. Such a result is consistent with the observed hydrogen hyperfine splittings in both central and peripheral lines. Hydrogen atoms *A* and *B* both only produce the selenium component labeled as Si-NL61. From this coincidence it is concluded that the *A* and *B* hydrogen atoms belong to a center with equal selenium hyperfine interaction. This converges to the conclusion that the Si-NL61 center has the two inequivalent hydrogen atoms *A* and *B* as its components. In a short summary, this latter conclusion is based on the equal *g* tensor of *A* and *B* hydrogen centers as revealed by FSE, the equal selenium hyperfine interaction as also indicated in FSE, and, moreover, the equal intensity ratio between *A* and *B* ENDOR lines in many

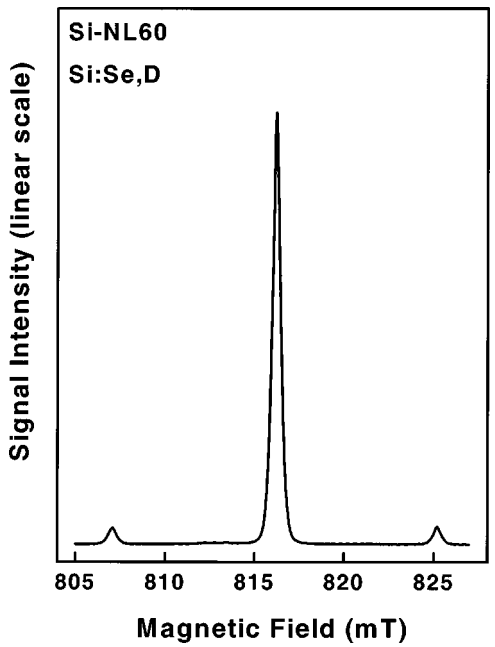

FIG. 9. EPR spectrum of deuterated sample doped with natural selenium, containing 7.6% ^{77}Se; only spectrum Si-NL60 is observed. The intensity ratio between the central line and two hyperfine lines is about 12:1. Temperature $T=4.2$ K, microwave frequency $f=22.7940$ GHz, and magnetic field $B\|\langle 100\rangle$.

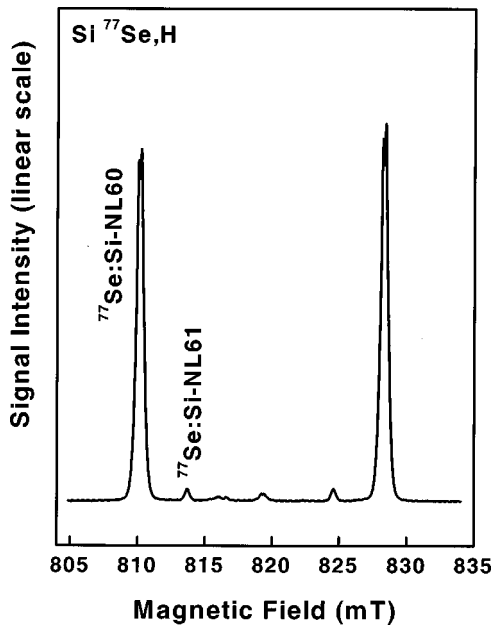

FIG. 10. EPR spectra Si-NL60 and Si-NL61 observed in a hydrogenated sample doped with selenium enriched to 99.1% in ^{77}Se. The central component corresponding to $m_I=0$ is almost absent; all intensity is in the hyperfine lines with $m_I=-\frac{1}{2}$ and $m_I=+\frac{1}{2}$. The spectrum was measured at $T=4.2$ K, $f=22.8777$ GHz, and $B\|\langle 100\rangle$.

samples made with varying quenching rates. The hyperfine interaction for the *A* hydrogen atom is some 8% smaller than that for the *B* atom.

C. Selenium identification

No ENDOR experiments were performed on the selenium nucleus. Conclusions about its presence are entirely based on the correlation between the resonance intensities and the abundance and nuclear spin of the ^{77}Se isotope. As ^{77}Se has a nuclear spin $I=\frac{1}{2}$, a twofold splitting is characteristic and required for its hyperfine structure. Figure 9 shows the EPR spectrum of a deuterated sample doped with natural selenium, containing 7.6% of ^{77}Se, and quenched very rapidly. Only the Si-NL60 spectrum was generated. The intensities of two hyperfine lines at around 807 and 825 mT together satisfy the expected ratio of 1:12 compared with the central line for the presence of one selenium atom. In passing it may be noted that in this sample with only the Si-NL60 spectrum and deuterium, rather than hydrogen, the central line became narrow and without structure. Also the twofold splitting of the selenium hyperfine lines as characteristic for hydrogen, and apparent in Fig. 1, is absent. The proper intensity ratio stays to be observed for all samples with a mixed presence of the Si-NL60 and Si-NL61 spectra. Therefore, for Si-NL61 a single selenium atom must also be present. Further substantiation of the conclusion is derived from the spectra observed in samples doped with selenium enriched to 99.1% in ^{77}Se. In such spectra (an example is given in Fig. 10), the central component has disappeared; all intensity has moved in equal proportion to the lines with $m_I=+\frac{1}{2}$ and $-\frac{1}{2}$. If two equivalent or inequivalent selenium atoms were present in the Si-NL60 or Si-NL61 centers, the spectra would have been essentially different. In the former case the centers produce a triple-line structure with an intensity ratio 1:2:1. As this is not observed the spectra do not correspond to a hydrogenated selenium pair, even though such pairs were present before hydrogen introduction.

D. Spin-Hamiltonian analysis

Following the qualitative description of the spectra, the quantitative spectroscopic analysis is based on the energy levels of the spin system. For both centers the electronic spin is $S=\frac{1}{2}$ due to a single unpaired electron spin, and the nuclear spin is $I=\frac{1}{2}$ for hydrogen, $I=1$ for deuterium, $I=\frac{1}{2}$ for isotope mass 77 of selenium, and $I=0$ for other selenium isotopes. The suitable form of the spin Hamiltonian,

$$\mathcal{H}=+\mu_B\mathbf{B}\cdot\mathbf{g}\cdot\mathbf{S}+\mathbf{S}\cdot\mathbf{A}_{Se}\cdot\mathbf{I}_{Se}+\Sigma\mathbf{S}\cdot\mathbf{A}_{H/D}\cdot\mathbf{I}_{H/D}$$
$$-\Sigma(g_n)_{H/D}\mu_N\mathbf{B}\cdot\mathbf{I}_{H/D}+\Sigma\mathbf{I}_D\cdot\mathbf{Q}_D\cdot\mathbf{I}_D, \quad (1)$$

has as a leading term the Zeeman energy of the electron, followed by the hyperfine interaction of the electron with selenium and one or two hydrogen/deuterium nuclei. The last two, purely nuclear, terms, the Zeeman energy and quadrupole energy, are required only for the ENDOR spectroscopy. The coupling tensors $\mathbf{g}$, $\mathbf{A}_{Se}$, $\mathbf{A}_{H/D}$, and $\mathbf{Q}_D$ all have the trigonal form. Results of computer fitting of data using the above Hamiltonian are collected in Table I. For comparison, the constants for the assumed similar centers Si-NL54 and Si-NL55 are given as well.

IV. DISCUSSION

A. Defect geometry

From experiments the trigonal symmetry of the Si-NL60 and Si-NL61 centers seems to be unambiguously established.

TABLE I. Spin-Hamiltonian parameters of Eq. (1) for the trigonal Si-NL60 and Si-NL61 centers obtained by computer fitting to experimental angular dependence data. g Tensor principal values are based on FSE measurements, selenium hyperfine interaction on EPR, and hydrogen/deuterium hyperfine and quadrupole interactions on ENDOR. Corresponding values for the sulfur-hydrogen spectra Si-NL54 and Si-NL55 are included for comparison (Refs. 15 and 16)

Parameter	Si-NL60	Si-NL61	Si-NL54	Si-NL55	Unit
Symmetry	trigonal	trigonal	trigonal	trigonal	
S	$\frac{1}{2}$	$\frac{1}{2}$	$\frac{1}{2}$	$\frac{1}{2}$	
$g_{\parallel}$	$1.966\,35 \pm 0.000\,05$	$1.996\,27 \pm 0.000\,05$	1.998 86	1.998 23	
$g_{\perp}$	$1.994\,59 \pm 0.000\,05$	$1.995\,12 \pm 0.000\,05$	2.001 26	1.999 74	
$(A_{\parallel})_{\mathrm{Se/S}}$	535.6 ± 2.5	321.5 ± 2.5	143.1	124	MHz
$(A_{\perp})_{\mathrm{Se/S}}$	495.3 ± 2.5	296.8 ± 2.5	137.7	117.9	MHz
$(A_{\parallel})_{\mathrm{H,1}}$	6.782 ± 0.01	1.060 ± 0.01	6.281	5.801	MHz
$(A_{\perp})_{\mathrm{H,1}}$	6.603 ± 0.01	0.816 ± 0.01	3.936	5.500	MHz
$(A_{\parallel})_{\mathrm{H,2}}$		1.020 ± 0.01			MHz
$(A_{\perp})_{\mathrm{H,2}}$		0.735 ± 0.01			MHz
$(A_{\parallel})_{\mathrm{D}}$	1.017 ± 0.005		0.959	0.867	MHz
$(A_{\perp})_{\mathrm{D}}$	0.990 ± 0.01		0.591	0.823	MHz
$(Q_{\parallel})_{\mathrm{D}}$	-0.032 ± 0.005		-0.048	-0.038	MHz
$(Q_{\perp})_{\mathrm{D}}$	$+0.016 \pm 0.005$		$+0.024$	$+0.019$	MHz

As the centers contain one selenium this atom must be situated on the ⟨111⟩ axis. The observed ⟨111⟩-axial symmetry of the hyperfine interaction with ^{77}Se confirms this statement. Selenium atoms occupy a substitutional site in silicon, either in their single isolated form or in a Se_2 pair. Also, in complexed form with Cu, the selenium atom stays on the lattice site. This situation is assumed to be true as well for the selenium-hydrogen complexes as observed in this experiment. Also, for hydrogen/deuterium atoms, a ⟨111⟩-axial symmetry of their hyperfine interaction is measured. This implies that these atoms must find their position on a ⟨111⟩ axis passing through the substitutional selenium atom. With one selenium atom on a substitutional site the center cannot have inversion symmetry. It follows that the hydrogen shells contain one atom. The hyperfine interactions A, B, and C thus each correspond to single hydrogen atoms. On can distinguish several possibilities for their sites: a bond-centered site between selenium and a neighboring silicon atom; an antibonding site with respect to selenium; an antibonding site with respect to silicon; or a site at larger distance from selenium along the ⟨111⟩ defect axis. Figure 11 illustrates some possibilities, all with the point-group symmetry $3m(C_{3\nu})$. The main question to be answered about atomic structure is on the position of the hydrogen atom(s) along the ⟨111⟩ axis. The main question for the electronic structure is whether the hydrogenated centers still are electrically active.

B. g tensor

The g values of the sulfur-hydrogen and selenium-hydrogen complexes, given in Table I, show small deviations only from the free-electron value $g_e = 2.0023$. These deviations are due to admixture of orbital momentum in the ground state by the spin-orbit interaction. As the effects are small they can be calculated by perturbation theory. A simple formula expresses the principal values g_i of the g tensor as

$$g_i = g_e - 2\lambda \Sigma_{n \neq 0} \langle 0|L_i|n\rangle\langle n|L_i|0\rangle/(E_n - E_0), \qquad (2)$$

with $i = 1$, 2, and 3.[26] Application of the formula in a practical case is a formidable task as interactions between ground state $|0\rangle$ and several excited states $|n\rangle$ have to be taken into account. So far, a calculation yielding excellent agreement with experimental values has only been reported for electrons in a conduction-band minimum.[27] Avoiding the detailed calculation of matrix elements and energies E_n, expression (2) can be the starting point for a semitheoretical treatment of the g tensor problem for certain series of defects with similar structures. If the defect wave function is of an extended character, the spin-orbit coupling constant $\lambda \approx 20$ meV for silicon $3p$ orbitals[28] will be applicable. The summation in Eq. (2) is replaced by an average constant assumed to be equal for all impurities in the series. In such a case the g value will depend only on the defect electron energy in its ground state E_0. Using this approach the g values for chalcogen donor impurities were related to the ionization energies of these deep double donors.[29] Results are illustrated in Fig. 12. Also included in this figure are data for the single substitutional donors P, As, and Sb,[30] and for some species of the thermal double donor TDD^+.[31] In understanding the substantial differences in the empirical relations, one must appreciate basic differences in the centers: deep and shallow electronic states; neutral single and ionized double donors; and cubic, trigonal and orthorhombic symmetries resulting in different sums of matrix elements of the orbital momentum operator. g Values of the sulfur- and selenium-hydrogen centers are indicated in Fig. 12 as well. It does not appear to be possible to estimate their ionization energies this way.

For shallow donors with a ground-state level close to the conduction band, one may expect the conduction band states to have a larger effect than the energetically more remote valence bands. With $\lambda \approx 20$ meV, an average $E_n - E_0 \approx 1.5$ eV (Ref. 29) and $0 < \langle 0|L_i|n\rangle\langle n|L_i|0\rangle \ll 1$, a small

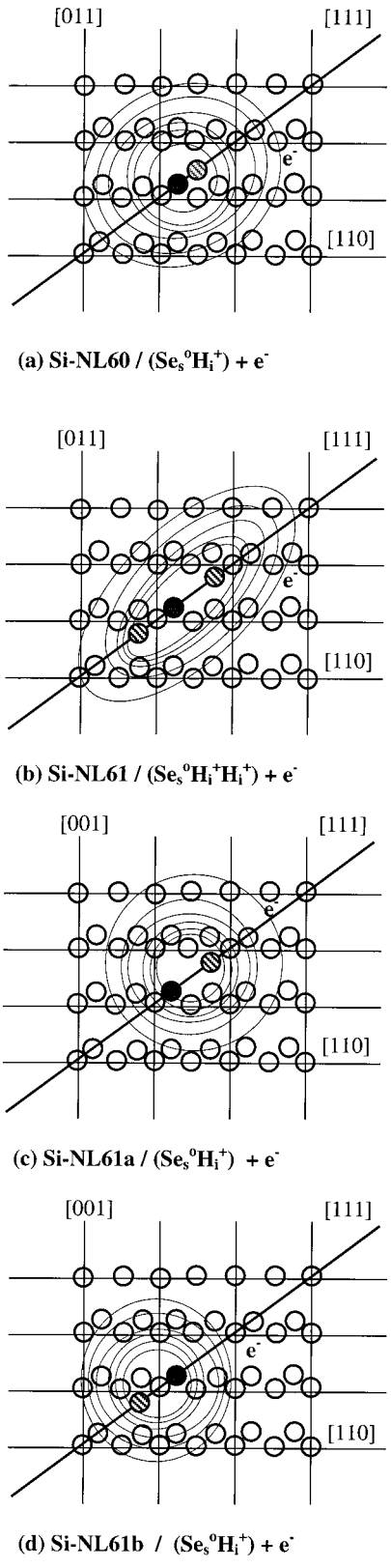

FIG. 11. Atomic structure models illustrating possible sites for hydrogen in the selenium-hydrogen complexes; the bond-centered site is not considered. Silicon ○, selenium ●, and hydrogen ⊖. (a) Model for the Si-NL60 center, (b) and [(c) and (d)] alternative models for center Si-NL61. All models have the point-group symmetry $3m(C_{3v})$.

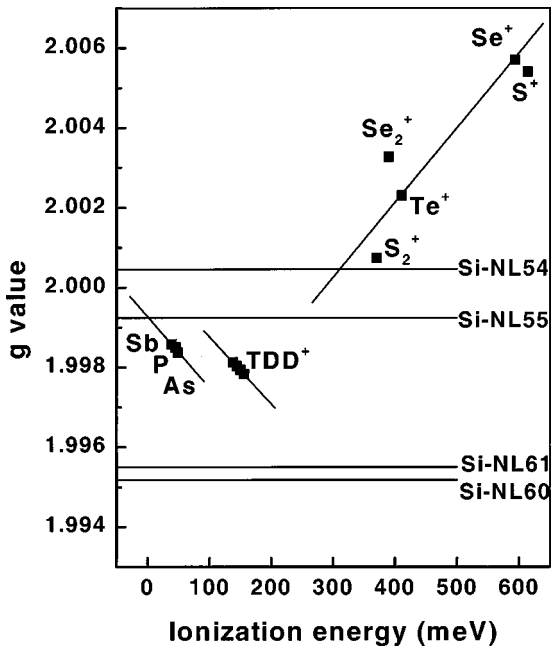

FIG. 12. Zeeman splitting factors g for the chalcogen double donors S^+, Se^+, and Te^+ in silicon vs the ionization energy (Ref. 29). Data for the single substitutional donors P, As, and Sb (Ref. 30), for some species of the thermal double donor TDD^+ (Si-NL8) (Ref. 31), for the sulfur-hydrogen centers Si-NL54 and Si-NL55 (Ref. 15), and for the selenium-hydrogen centers (present work) are included as well.

negative g shift follows from Eq. (2). An empirical classification of defects after their g values, initiated by Lee and Corbett[32] and later discussed by Sieverts in more detail,[33] confirms the validity of the prediction. Paramagnetic centers known as effective mass donors all have their g values slightly below g_e. It may therefore be concluded that the SH centers Si-NL54 and Si-NL55 and the SeH centers Si-NL60 and Si-NL61 are also in this category of donors with not too deep ionization energies. Again, no estimate can be made of the ionization energies.

One more aspect of the g tensors of Si-NL60 and Si-NL61 must be discussed. Center Si-NL61 was identified as a selenium–two-hydrogen complex. The threefold independent evidence for the model is the equal ^{77}Se hyperfine interaction linked to the two hydrogen atoms revealed in FSE, the equal g tensor of the center related to the two hydrogen atoms also determined by FSE measurements, and the invariable ratio of the two hydrogen ENDOR intensities over several samples. Having two hydrogen atoms the magnetic resonance of the Si-NL61 center is observed in an ionized state. Contrary to this situation, the magnetic resonance of Si-NL60 will be observed in its neutral state. In view of the presented classification of centers, one would expect a clear difference in their g tensors. However, the g tensors of the two centers are remarkably close. In view of this fact the interpretation of the Si-NL61 spectrum as arising from two different one-hydrogen centers cannot be ruled out. It might be the case that two very similar SeH pairs, indistinguishable by their EPR spectrum, exist. In this respect the observation in optical absorption of two SH pairs with very close ionization energies of 135.07 and 135.45 meV might be relevant information.[14] Two different EPR spectra related to these

TABLE II. Parameters related to the analysis of hyperfine interactions of the Si:Se,H spectra Si-NL60 and Si-NL61, and of the Si:S,H spectra Si-NL54 and Si-NL55. The localization on the impurities is given by η^2, and the fraction of *s*- and *p*-type wave functions by α^2 and β^2, respectively. Nuclear *g* values from Ref. 25, are $g_n=1.0682$ for ^{77}Se, $g_n=0.4289$ for ^{33}S, $g_n=5.58556$ for ^{1}H, and $g_n=0.85742$ for ^{2}D.

Parameter	Si-NL60	Si-NL61		Si-NL54	Si-NL55	Unit
Nucleus	^{77}Se	^{77}Se		^{33}S	^{33}S	
a	508.7	305.0		139.5	119.9	MHz
b	13.4	8.2		1.8	2.0	MHz
η^2	5.67	3.43		5.89	5.54	%
α^2	52	51		70	64	%
β^2	48	49		30	36	%
Nucleus	^{1}H	^{1}H	^{1}H	^{1}H	^{1}H	
a	6.663	0.897	0.830	4.718	5.600	MHz
b	0.060	0.081	0.095	0.782	0.100	MHz
η^2	0.47	0.063	0.058	0.33	0.39	%
Nucleus	^{2}D			^{2}D	^{2}D	
a	0.999			0.714	0.838	MHz
b	0.009			0.123	0.015	MHz
η^2	0.46			0.33	0.38	%

infrared centers were not reported in previous studies of the sulfur hydrogenation.[15] There could exist a parallel with the oxygen-related thermal donor centers, where species can be identified in infrared absorption but are not separable in magnetic resonance at the usual frequencies.

C. Hyperfine interaction tensor

From the observed hyperfine interaction constants, the wave function at the sites of the magnetic nuclei can be calculated. If a full set of hyperfine interaction data is available, a detailed map of the wave function of the defect electron can be constructed. For the present case of hydrogenated selenium centers the unpaired defect electron experiences hyperfine interactions with the magnetic nuclei ^{77}Se, ^{1}H/^{2}D, and ^{29}Si; these will be discussed successively.

On the site of a selenium atom the wave function of the defect electron can be written as a linear-combination-of-atomic-orbitals (LCAO) expression

$$\psi=\eta[\alpha\varphi_{4s}(\vec{r})+\beta\varphi_{4p}(\vec{r})], \tag{3}$$

where $\varphi_{4s}(\vec{r})$ and $\varphi_{4p}(\vec{r})$ represent the atomic $4s$ and $4p$ wave functions of selenium, respectively. The localization of the defect electron at the selenium site is given by η^2, and the *s* and *p* characters of the wave function are measured by parameters α and β. A normalization condition $\alpha^2+\beta^2=1$ is imposed. The spherically symmetric $4s$ function leads to an isotropic hyperfine interaction, known as the Fermi contact interaction. The hyperfine interaction constant *a* is related to the wave function by

$$a=(2/3)\mu_0 g\mu_B(g_n)_{Se}\mu_N\eta^2\alpha^2|\varphi_{4s}(0)|^2. \tag{4}$$

From the $4p$ orbital on the selenium site, an axially symmetric hyperfine interaction will result with a strength *b* related to the wave function by

$$b=(2/5)(1/4\pi)\mu_0 g\mu_B(g_n)_{Se}\mu_N\eta^2\beta^2\langle r^{-3}\rangle_{4p}. \tag{5}$$

On the principal directions of the trigonal center the hyperfine interaction tensor will be specified by its parallel principal value $A_\parallel$ and perpendicular value $A_\perp$. These follow from the components in the $\langle 100\rangle$ Cartesian coordinate system by

$$A_\parallel=a+2b \tag{6}$$

and

$$A_\perp=a-b. \tag{7}$$

The measured hyperfine interaction data for the ^{77}Se isotope (see Table I) were analyzed following this schedule. In these calculations the atomic wave function quantities were taken as $|\varphi_{4s}(0)|^2=137.73\times10^{30}\,\mathrm{m}^{-3}$ and $\langle r^{-3}\rangle_{4p}=81.32\times10^{30}\,\mathrm{m}^{-3}$.[34] Atomic wave function coefficients η, α, and β are given in Table II. The localization on the selenium atoms is found to be $\eta^2\approx5\%$ for the center Si-NL60 and $\eta^2\approx3\%$ for Si-NL61. Such a result is intermediate between the localizations $\eta^2\approx1\%$ for the shallow substitutional single donors P, As, and Sb in silicon and $\eta^2\approx9\%$ for the double donors S^+, Se^+, and Te^+. The wave function has a substantial *s*-type character which is invariant under all operations of the $3m$ symmetry group of the center. This indicates the A_1 symmetry type for the ground state.

Following the same procedure the isotropic part of the hyperfine interaction with the hydrogen isotopes ^{1}H with $I=\frac{1}{2}$ and ^{2}D with $I=1$, can be analyzed. Using $|\varphi_{1s}(0)|^2=2.15\times10^{30}\,\mathrm{m}^{-3}$, localizations η^2 below 0.5%, as given in Table II, are obtained. Interactions as observed for the proton and the deuteron always scale properly according to the nuclear *g* values, i.e., no indications of a hyperfine anomaly are present. Analysis of the anisotropic part requires a different approach. An LCAO description using the lowest-lying *p* orbital of hydrogen is inappropriate as the energy of this state is too high to be occupied. Contrary to the previous cases, the hyperfine interaction does not arise from orbitals centered on the site itself, but on spin density on neighboring sites. By an equation similar to Eq. (5), one calculates that for a nearest-neighbor distance in the silicon crystal, $r=0.235\,\mathrm{nm}$, and for a fully occupied orbital the anisotropic interaction on the ^{1}H nucleus is 6.10 MHz. Taking the model

of hydrogen located on an interstitial T site at nearest distance to the selenium atom, as for Si-NL60 in Fig. 11(a), the 5% spin density on selenium will have an interaction strength of $b=300$ kHz with hydrogen. This is more than observed for the SeH centers and sulfur center Si-NL55. Hydrogen on the interstitial T site will also be surrounded by three equivalent silicon neighbors at tetraeder corners, all at a distance of 0.235 nm. The spin density on these silicon neighbors will make contributions to the hydrogen hyperfine pointing in the opposite $\langle 111\rangle$ direction. Also on a more general site along the $\langle 111\rangle$ axis, T site or not, near to selenium or not, the hydrogen atom will be surrounded on all sides by silicon neighbors carrying spin densities of similar magnitude. Altogether, the anisotropic part of the hyperfine interaction on the hydrogen may well be accounted for by spin density on neighbor sites. The situation is different for sulfur center Si-NL54, which has a much larger anisotropic hyperfine interaction, the factor 8 difference from Si-NL55 suggesting a twice-smaller distance of the remote spin density. This is provided in an obvious manner if the hydrogen occupies the bond-centered (BC) interstitial site between S and Si. This is the preferred model for the Si-NL54 center. The absence of the strong anisotropic interaction for Si-NL60 and Si-NL61 is an indication that the BC site is not available as a hydrogen position in the SeH pairs. The spin density is nearly zero in the hydrogen atomic cell. Apparently the spin and charge of the electron introduced by the neutral hydrogen atom disappeared from the cell when the complex with the selenium was formed. The atomic cell around hydrogen carries one unit of positive charge.

No hyperfine interactions with ^{29}Si were observed. These must be present as the natural silicon crystals contain 4.7% of this magnetic isotope with $I=\frac{1}{2}$. Their absence is not due to their small intensity, which in the minimum case of a shell with one silicon atom is $\approx$2.5% of the corresponding $I=0$ resonance. The signal-to-noise ratio of recording the spectra was sufficiently high to observe also the small hyperfine satellites; see, e.g., Figs. 8–10. Most probably all ^{29}Si hyperfine interactions are so weak that the doublet splittings occur within the line width of one composite line. A typical linewidth (full width at half maximum) in the EPR of 0.5 mT corresponds to a hyperfine constant $a\approx 15$ MHz and a localization of 0.33% of a silicon $3s$ orbital. In order to account for the whole wave function it must be spread over at least 300 atom sites. A spherical volume with a radius of 1 nm is required to contain this number of atoms. The absence of resolved ^{29}Si hyperfine structure thus indicates an extended wave function, typical for an electron bound in a long-range Coulomb potential.

The model emerging from the wave-function mapping by hyperfine measurements is that of a $(\mathrm{Se}_s)^0(\mathrm{H}_1)^+$ impurity pair, giving the center a trigonal core structure. The positively charged core is surrounded by an electron with a typical effective-mass wave function radius around 1 nm. The probability of the defect electron is distributed over hundreds of sites, with that on the selenium atom somewhat enhanced by a central cell correction.

D. Quadrupole interaction tensor

The quadrupole term represents the energy of the nuclear electric quadrupole moment in an inhomogeneous electric field on the site of the nucleus. It only occurs for nuclei with spin $I\geqslant 1$ and, therefore, in the present study, only the deuteron is available as suitable nucleus for monitoring electric-field and corresponding charge distributions in the defect environment. Electric charges in a complex center are usually divided into charge on the site of the nucleus itself and those on neighboring sites. In the former category are core electrons in inner full electron shells, electrons in valence states, and unpaired defect electrons. Due to their proximity to the nucleus, these interactions usually dominate over those from more distant charge unbalance. The present case of the deuteron in the SeH center, however, is exceptional as none of these electrons exist in the ionized D^+, a unique feature of the element hydrogen. The only charge present on the deuteron is in a symmetric $1s$ orbital, and does not create any electric-field gradient. The quadrupole effect is therefore made by distant charges and will be small. In previous studies of the sulfur-hydrogen centers Si-NL54 and Si-NL55 this was confirmed as indeed the quadrupole interactions with deuterium, of order 20 kHz, were small compared to those of sulfur, as measured on isotope ^{33}S with $I=\frac{3}{2}$ and a quadrupole energy near 3 MHz. Taking into account that the quadrupole moment for ^{33}S, $q_S=-55\times 10^{-30}$ m^2,[25] is larger than that of the deuteron, $q_D=2.86\times 10^{-30}$ m^2,[25] one still concludes that the electric-field gradients on the hydrogen site are smaller by an order of magnitude. A unit charge e at a distance r from the nucleus creates a radial electric-field gradient of

$$d^2V/dr^2=2e/4\pi\varepsilon_0 r^3, \tag{8}$$

and an off-diagonal quadrupole parameter

$$q=(1/4\pi\varepsilon_0)[e^2q_D/2I(2I-1)](1/r^3). \tag{9}$$

For a full electron charge at the nearest-neighbor distance $r=0.235$ nm parameter q will be 3.83 kHz. As this is some factor 4 smaller than the observed 16 kHz for Si-NL60, there must be considerable charge redistribution in the core of the center. An obvious possibility is the movement of the two electrons in the neutral sulfur double donor toward the positive hydrogen position. A shift of two electrons by 0.07 nm would be required to account for the quadrupole effect as observed.

V. CONCLUSION

By magnetic resonance (EPR, ENDOR, and FSE), two spectra, labeled Si-NL60 and Si-NL61, related to SeH complexes in silicon were detected. Their atomic and electronic structures were characterized by their g tensors, hyperfine interactions, and nuclear quadrupole effect. The selenium-hydrogen complexes have the trigonal symmetry, with all impurities on a $\langle 111\rangle$ crystal axis, selenium on a substitutional site, hydrogen atoms on interstitial sites. For the Si-NL60 center a single hydrogen position on the Se or Si antibonding sites is preferred. The Si-NL61 center can correspond to two very similar one-Se–one-H centers or to one $\mathrm{SeH}_\alpha\mathrm{H}_\beta$ center with two slightly inequivalent hydrogen sites. The ambiguity is not finally resolved. To first approxi-

mation the core of the center consists of a neutral selenium atom and a positive hydrogen. Some transfer of charge is likely to occur resulting in a $Se^{+\delta}H^{+1-\delta}$ charged pair. An electron is electrostatically bound to this core in an extended orbit. The center resembles in its properties the shallow single or double donors which are well described by the effective-mass theory, with an additional central cell potential accounting for the ground-state properties.

[1] E. Janzén, R. Stedman, G. Grossmann, and H. G. Grimmeiss, Phys. Rev. B **29**, 1907 (1984).

[2] H. G. Grimmeiss and M. Kleverman, *Properties of Silicon*, EMIS Datareviews Series No. 4 (The Institution of Electrical Engineers, London, 1988), p. 240.

[3] P. Wagner, C. Holm, E. Sirtl, R. Oeder, and W. Zulehner, Festkörperprobleme **XXIV**, 191 (1984).

[4] G. W. Ludwig, Phys. Rev. **137**, A1520 (1965).

[5] O. F. Schirmer, Physica B & C **116**, 306 (1983).

[6] L. Jeyanathan, G. Davies, E. C. Lightowlers, M. Singh, H. J. Sun, B. Ittermann, S. S. Ostapenko, W. A. Barry, P. Mason, and G. D. Watkins, Mater. Sci. Forum **143–147**, 1167 (1994).

[7] W. M. Chen, E. Janzén, B. Monemar, A. Henry, A. M. Frens, M. T. Bennebroek, and J. Schmidt, Mater. Sci. Forum **143–147**, 1179 (1994).

[8] P. W. Mason, H. J. Sun, B. Ittermann, S. S. Ostapenko, G. D. Watkins, L. Jeyanathan, M. Singh, G. Davies, and E. C. Lightowlers, Phys. Rev. B **58**, 7007 (1998).

[9] J. I. Pankove, D. E. Carlson, J. E. Berkeyheiser, and R. O. Wance, Phys. Rev. Lett. **51**, 2224 (1983).

[10] N. M. Johnson, C. Herring, and D. J. Chadi, Phys. Rev. Lett. **56**, 769 (1986).

[11] Y. Kamiura, N. Ishiga, and Y. Yamashita, Jpn. J. Appl. Phys. **36**, L1419 (1997).

[12] G. Pensl, G. Roos, C. Holm, E. Sirtl, and N. M. Johnson, Appl. Phys. Lett. **51**, 451 (1987).

[13] G. Pensl, G. Roos, P. Stolz, N. M. Johnson, and C. Holm, *Defects in Electronic Materials* (Materials Research Society, Pittsburgh, 1988), p. 241.

[14] R. E. Peale, K. Muro, and A. J. Sievers, Mater. Sci. Forum **65–66**, 151 (1990).

[15] I. S. Zevenbergen, T. Gregorkiewicz, and C. A. J. Ammerlaan, Phys. Rev. B **51**, 16 746 (1995).

[16] I. S. Zevenbergen, T. Gregorkiewicz, and C. A. J. Ammerlaan, Mater. Sci. Forum **196–201**, 855 (1995).

[17] P. Kaczor (unpublished).

[18] H. G. Grimmeiss, E. Janzén, H. Ennen, O. Schirmer, J. Schneider, R. Wörner, C. Holm, E. Sirtl, and P. Wagner, Phys. Rev. B **24**, 4571 (1981).

[19] S. Greulich-Weber, J. R. Niklas, and J.-M. Spaeth, J. Phys. C **17**, L911 (1984).

[20] J. R. Niklas and J. M. Spaeth, Solid State Commun. **46**, 121 (1983).

[21] R. Wörner and O. F. Schirmer, Solid State Commun. **51**, 665 (1984).

[22] A. B. van Oosten and C. A. J. Ammerlaan, Phys. Rev. B **38**, 13 291 (1988).

[23] S. Greulich-Weber, J. R. Niklas, and J.-M. Spaeth, J. Phys.: Condens. Matter **1**, 35 (1989).

[24] M. Sprenger, Ph.D. thesis, University of Amsterdam, 1986.

[25] G. S. Fuller, J. Phys. Chem. Ref. Data **5**, 835 (1976).

[26] M. H. L. Pryce, Proc. Phys. Soc. London **63**, 25 (1950).

[27] L. Liu, Phys. Rev. **126**, 1317 (1962).

[28] G. D. Watkins and J. W. Corbett, Phys. Rev. **121**, 1001 (1961).

[29] O. F. Schirmer and M. Scheffler, J. Phys. C **15**, L645 (1982).

[30] C. F. Young, E. H. Poindexter, G. J. Gerardi, W. L. Warren, and D. J. Keeble, Phys. Rev. B **55**, 16 245 (1997).

[31] R. Dirksen, F. Berg Rasmussen, T. Gregorkiewicz, and C. A. J. Ammerlaan, Mater. Sci. Forum **258–263**, 373 (1997).

[32] Y. H. Lee and J. W. Corbett, Phys. Rev. B **8**, 2810 (1973).

[33] E. G. Sieverts, Phys. Status Solidi B **120**, 11 (1983).

[34] J. R. Morton and K. F. Preston, J. Magn. Reson. **30**, 577 (1978).